Supporting Information for

Uniform doping of metal oxide nanowires using solid state diffusion

Joaquin Resasco[1], Neil P. Dasgupta[2,3], Josep Roque Rosell[4], Jinghua Guo[4], and Peidong Yang[2,5]*

[1]Department of Chemical Engineering and [2]Department of Chemistry, University of California, Berkeley, California 94720, United States. [3]Department of Mechanical Engineering, University of Michigan, Ann Arbor, Michigan 48109, United States. Advanced Light Source, Lawrence Berkeley National Laboratory, Berkeley, California 94720, United States. [5]Materials Sciences Division, Lawrence Berkeley National Laboratory, Berkeley, California 94720, United States

Table S1. EXAFS Curve Fitting Parameters

Path	R(Å)	N	σ^2(Å^2)	ΔE_0(eV)	S_0	R_f(%)
Mn-O	2.03	4	.00386	2.6576	0.8607	1.6
Mn-O	2.15	2	.00428			
Mn-Ti	3.30	4	.0104			
Mn-Ti	3.79	4	.0127			

The coordination number N was taken to be fixed for the crystalline material. S_0 and ΔE_0 were fit to the same value for all paths as they are properties of the central atom.

X-Ray Photoelectron Spectroscopy

Sample	**Source**	**Δ2p1/2 (eV)**	**Δ3s (eV)**
MnO	This work	6.0	6.1
	Ref S1	6.0	6.0
	Ref S2	5.4	6.1
Mn_2O_3	This work	10.1	5.2
	Ref S1	10.0	5.1
	Ref S2	10.5	5.4
MnO_2	This work	12.0	4.7
	Ref S1	11.8	4.5
	Ref S2	11.9	4.5
As deposited		10.75	5.3
Annealed		6.2	6.0

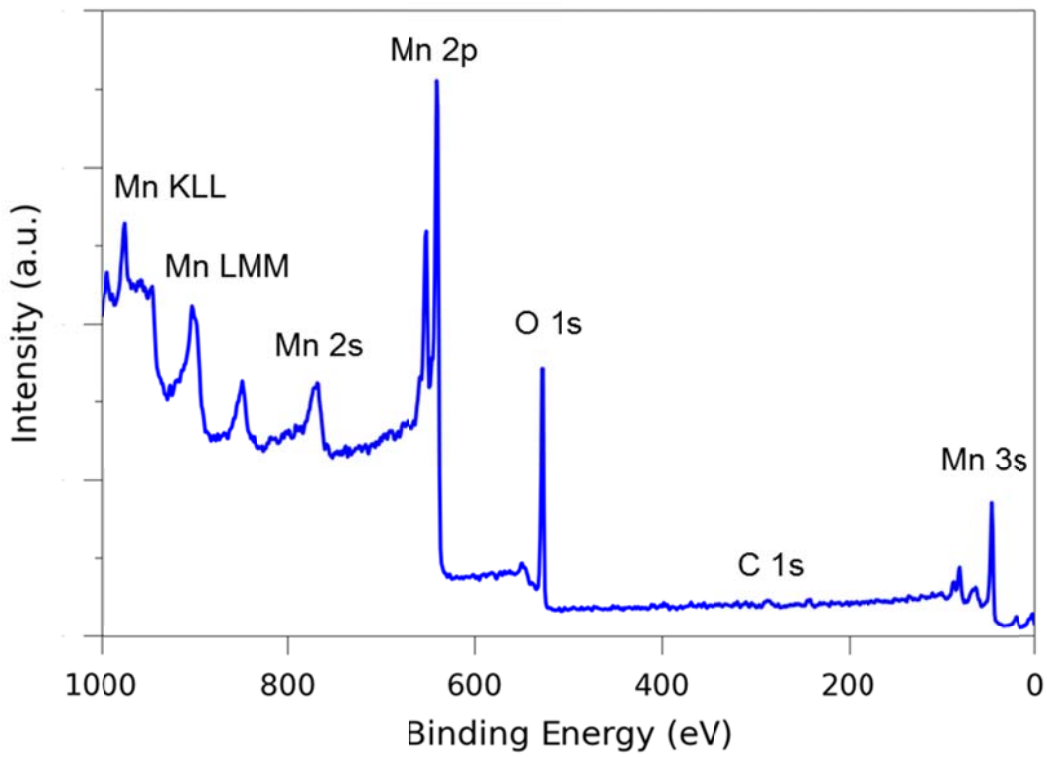

Figure S1: XPS survey spectra of MnO_x ALD films deposited using the Manganese bis(N,N'-diisopropylacetamidinate) following a 60 sec Ar sputter. The lack of carbon in the spectrum reflects the thermal stability of the amidinate precursor.

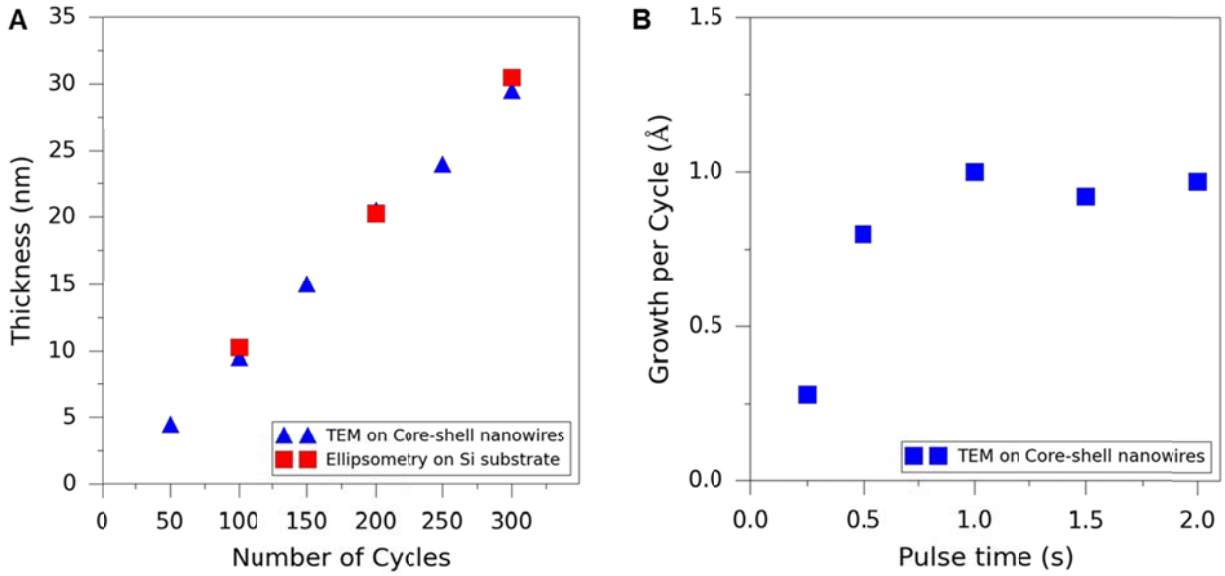

Figure S2: (A) Thickness of MnO_x ALD films measured by TEM and ellipsometry as a function of number of cycles. A linear growth rate of ~1.0 Å/cycle was observed. (B) Growth rate per cycle of MnO_x ALD films under increasing pulse time of the Mn amidinate precursor. Saturation was observed after 1.0 s.

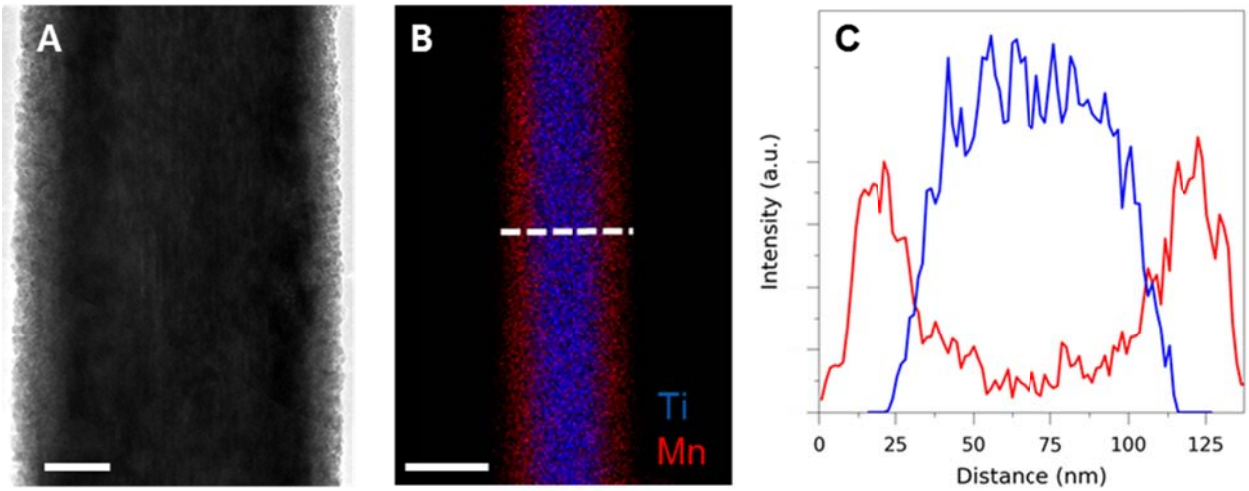

Figure S3: (A) TEM image of a core-shell $TiO_2|MnO_x$ nanowire after 100 cycles, showing a conformal coating. Scale bar is 20 nm. (B,C) STEM mode EDS mapping and corresponding line scan of core-shell nanowire after 200 cycles showing confinement of the Mn to the shell of the wire and the Ti in the core. Scale bar is 100 nm.

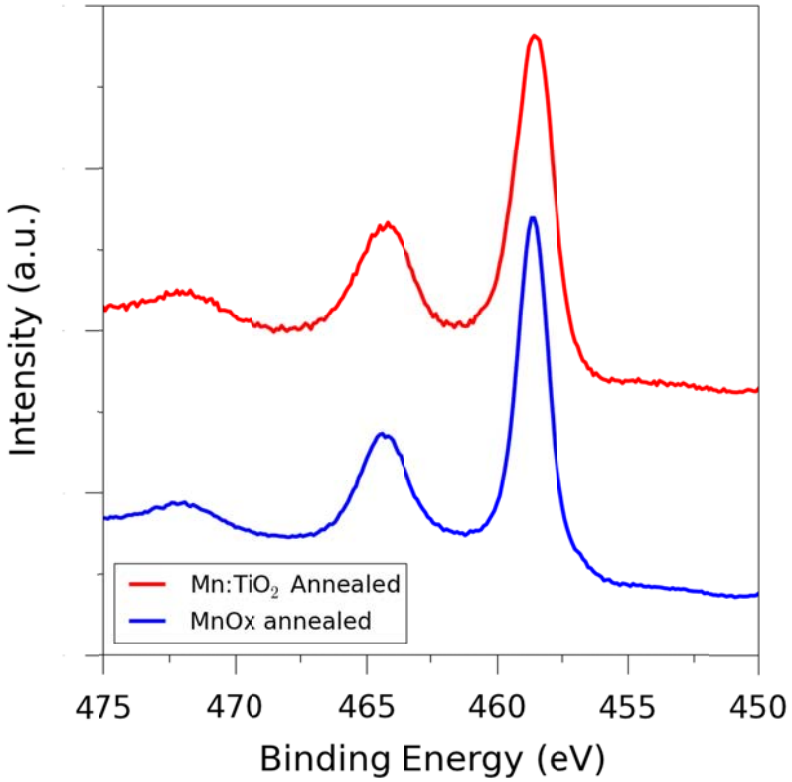

Figure S4: XPS spectra of the Ti 2p region, showing the binding energy and peak structure are unchanged before and after the conversion process.

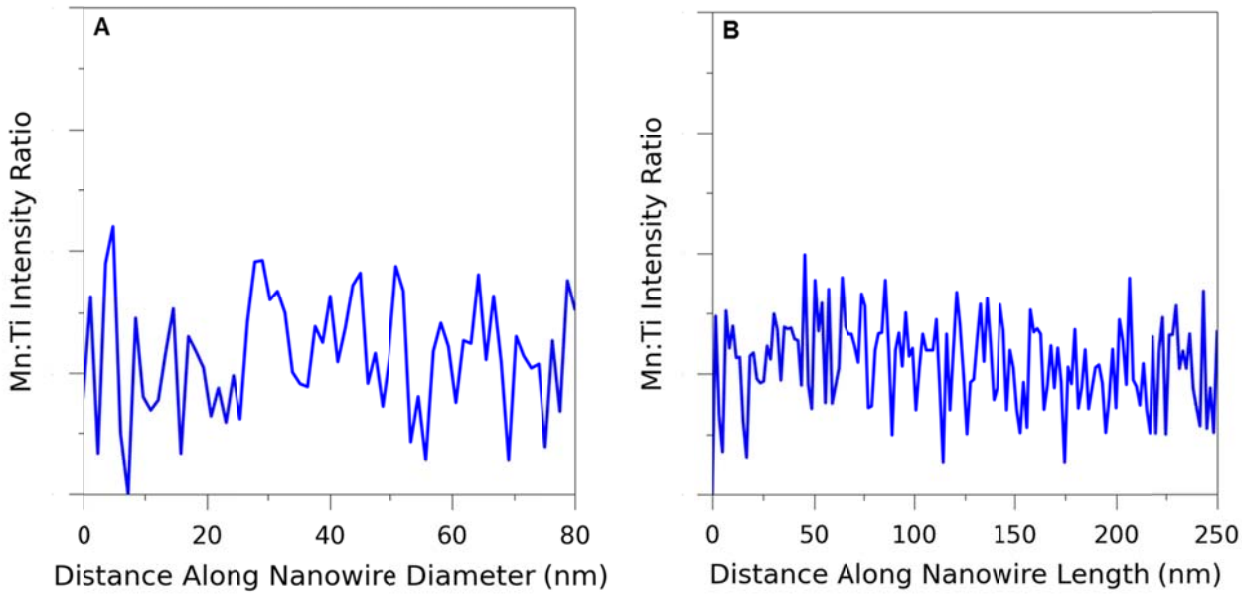

Figure S5: EDS line scans of Mn:TiO_2 nanowires showing the Mn:Ti intensity ratio across the diameter (A) and length (B) of the wire, indicating the homogeneous incorporation of the Mn dopant. Corresponding elemental maps are shown in Figure 1f and 1g.

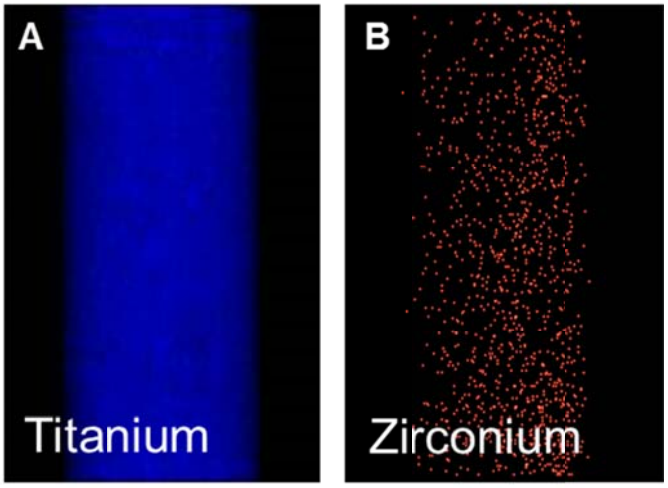

Figure S6: (A,B) STEM mode elemental maps of Ti and Zr in converted wire.

Calculation of Expected Mn Concentration

$$N_{Mn} = \frac{\pi(R_2^2 - R_1^2)\Delta L \rho_{MnO}}{MW_{MnO}} \qquad N_{Ti} = \frac{\pi R_1^2 \Delta L \rho_{TiO_2}}{MW_{TiO_2}}$$

$$Mn\ atomic\ percentage = \frac{N_{Mn}}{N_{Mn} + N_{Ti}} = \frac{\frac{(R_2^2 - R_1^2)\rho_{MnO}}{MW_{MnO}}}{\frac{(R_2^2 - R_1^2)\rho_{MnO}}{MW_{MnO}} + \frac{R_1^2 \rho_{TiO_2}}{MW_{TiO_2}}}$$

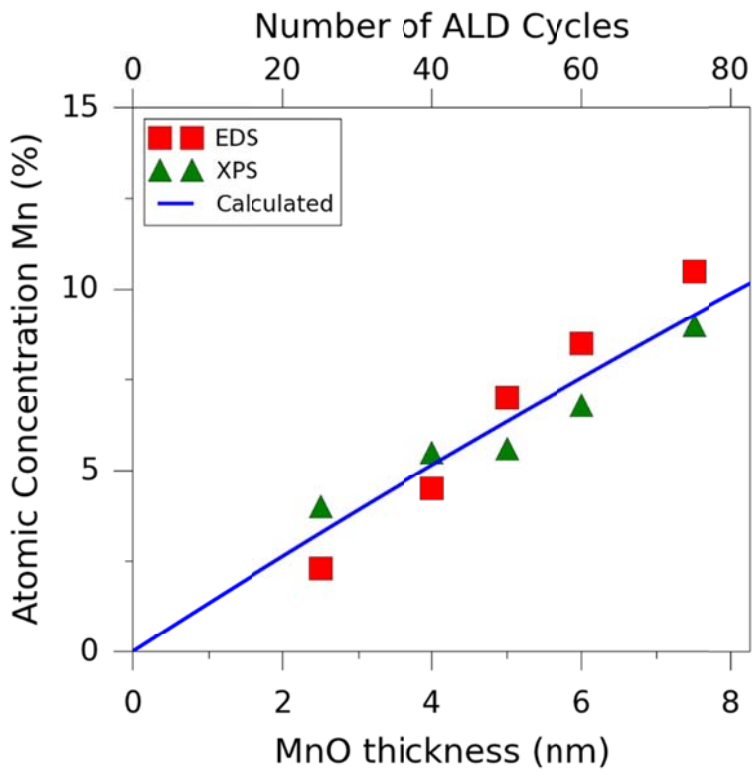

Figure S7: Measured and calculated atomic concentration of Mn in converted wires as a function of ALD film thickness.

Ternary $MnTiO_3$ Phase Formation

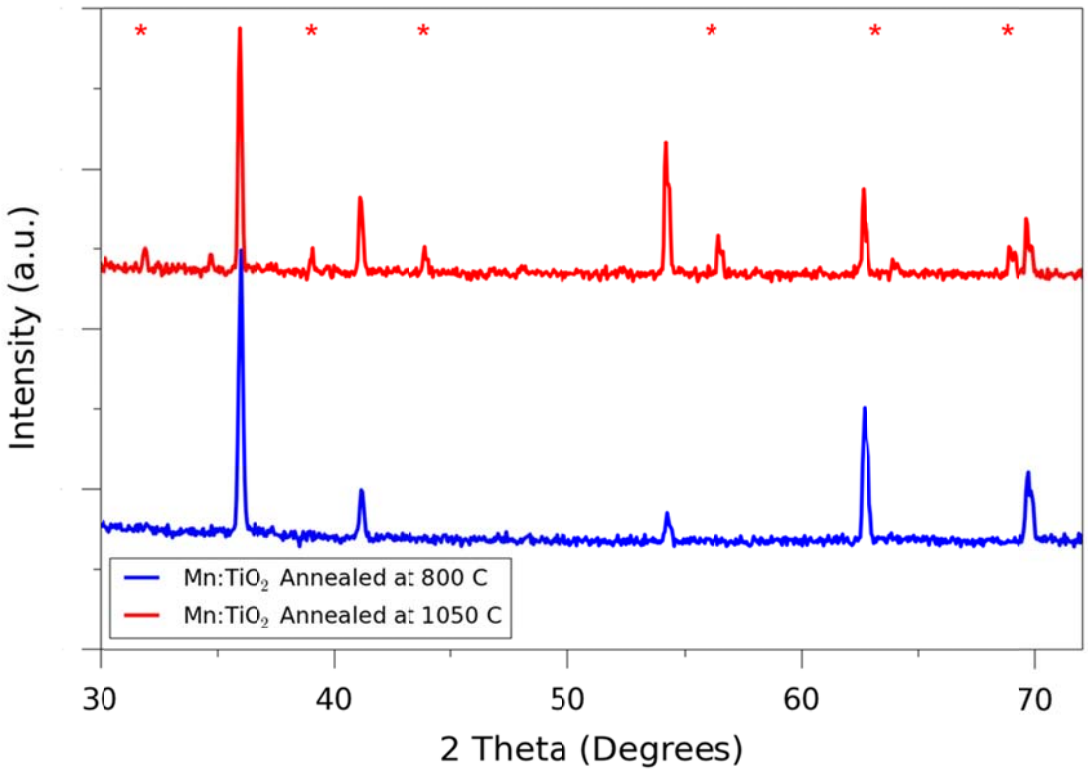

Figure S8: X-Ray Diffraction patterns for converted wire samples at different annealing temperatures. The ternary phase $MnTiO_3$ is formed at 1050°C. * indicates diffraction lines for $MnTiO_3$.

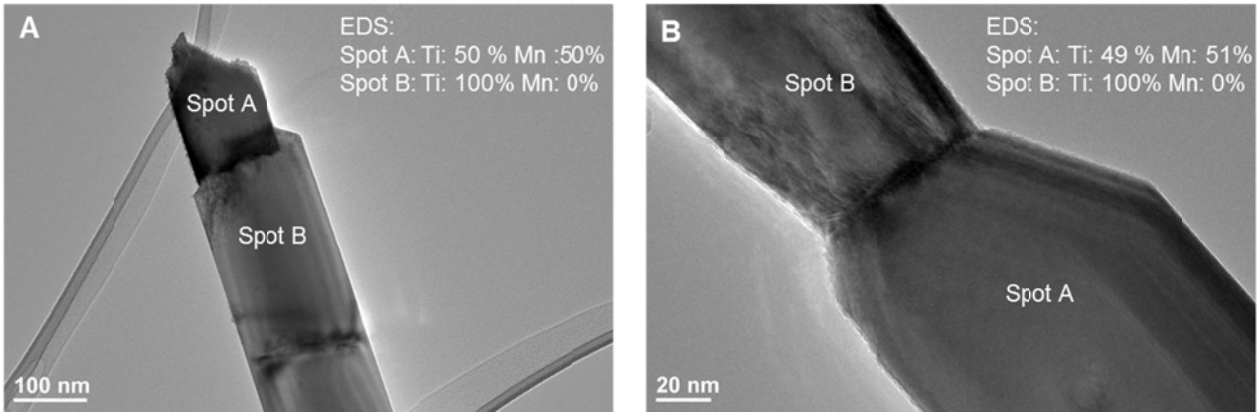

Figure S9: (A,B) TEM images of nanowires converted at 1050°C. Nanowires phase segregate to form axial segments of pure $MnTiO_3$ and TiO_2. Axial segmentation is likely due to high diffusion rates of Mn^{2+} along c-axis. EDS confirms relative stoichiometry of Mn and Ti in segments.

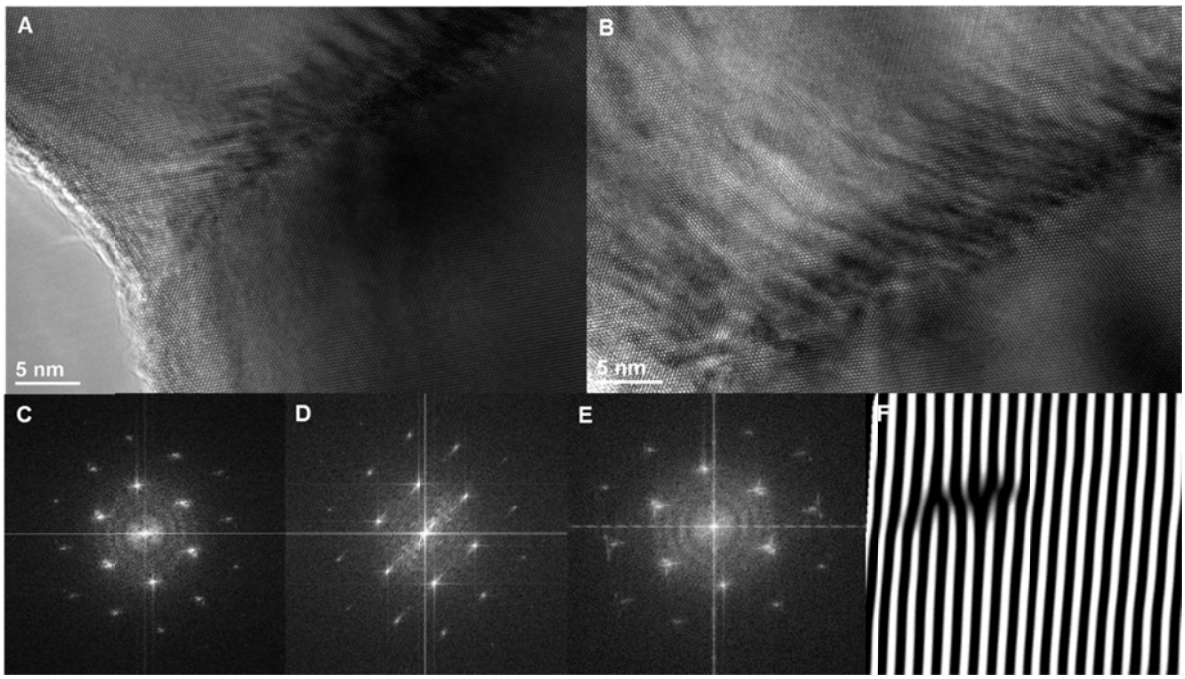

Figure S10: (A,B) HRTEM images of nanowires converted at 1050°C, showing the interface between $MnTiO_3$ and TiO_2. (C-E) FFTs of TiO_2 section, $MnTiO_3$ section, and interface respectively. (F) Moiré image shows epitaxial interface between $MnTiO_3$ $1\bar{1}0$ and TiO_2 001 which can form due to the similarity of the oxygen sublattice in the two structures. However, edge dislocations are observed at the interface.

Transient Diffusion of Mn in TiO_2 Nanowires

The transient diffusion of Mn in the TiO_2 nanowire can be described by Fick's Second Law:

$$\frac{\partial c_A}{\partial t} = D_{AB}\frac{\partial^2 c_A}{\partial x^2}$$

Where c_A is the concentration of Mn and x is the distance from the edge of the nanowire. The solution for diffusion into a finite medium solution can be obtained numerically and is available in for simple geometric shapes in Gurney-Lurie charts. The numerical solution would predict a more rapid conversion than the solution for a semi-infinite medium but otherwise similar diffusion profiles. Therefore as a simple approximation, the nanowire can be considered a semi-infinite medium to yield an analytical solution:

$$\frac{c_{As} - c_A}{c_{As} - c_{A0}} = \mathrm{erf}\left(\frac{z}{2\sqrt{D_{AB}t}}\right)$$

The surface concentration of Mn (c_{As}) can be taken as unity as the nanowire shell is manganese oxide. The initial concentration of Mn in the nanowire (c_{A0}) is zero.
From single crystal studies the diffusion coefficients of various transition metals in rutile TiO_2 at different partial pressures of oxygen are known.[3] The diffusion coefficients of interest here are those orthogonal to the c-axis, which are lower than those parallel to the c-axis. The diffusion coefficients were also measured to be substantially higher at low partial pressures of oxygen. The diffusion coefficient of Mn in TiO_2 is quite high: $1.1*10^{-10}$ cm^2/s at 900°C in air. As the diffusion distance is quite small as the nanowire diameter is ~100 nm, the nanowires readily become fully converted at high temperature.

To observe the transient diffusion behavior the conversion process was investigated at lower temperatures. The expected distribution of Mn for the semi-infinite medium solution at T=600°C is shown in Figure S11, assuming a diffusion coefficient of $2.7*10^{-12}$ cm^2/s for Mn diffusion orthogonal to the c-axis in an Ar environment. STEM elemental maps for incomplete conversion for different conversion times are shown in Figure S12. We see that at elevated temperatures the conversion is very rapid, and that the expected diffusion profiles are reproduced by the experimental data.

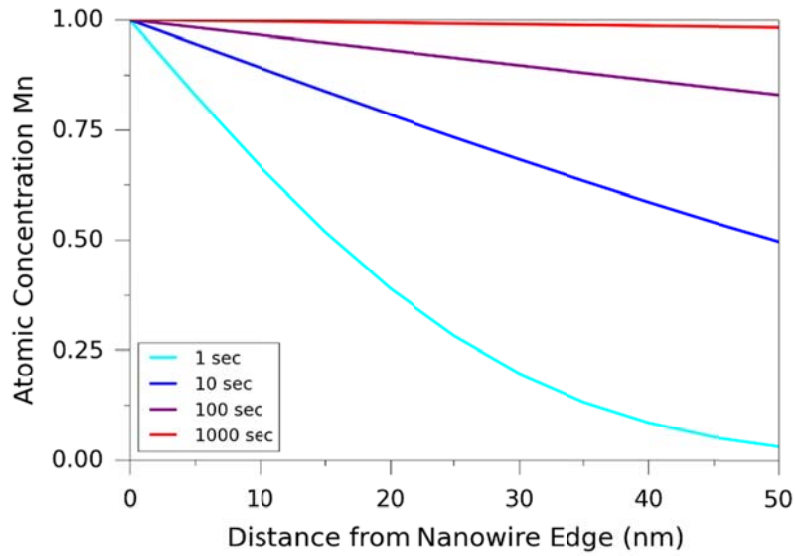

Figure S11: Mn distributions in the TiO_2 nanowire as a function of time for conversion at 600°C in an Ar environment. The nanowire is assumed to be a semi-infinite medium. The nanowire becomes fully converted in a relatively short conversion time.

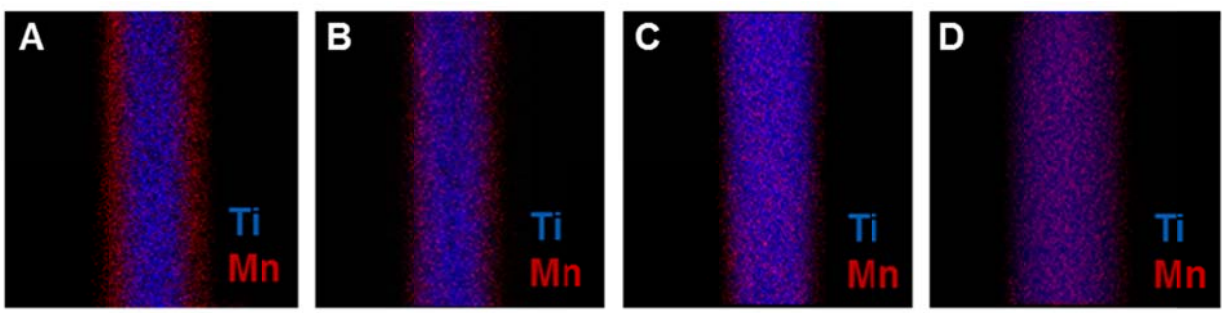

Figure S12: (A-D) STEM mode EDS elemental maps for transient conversion of nanowire after 0, 1, 10, and 100 min of conversion at 600°C in Ar.

Mechanism for Diffusion Process

From single crystal studies on metal ion diffusion in rutile TiO_2, the mechanism of diffusion is suggested to be dependent on the charge state of the ion. Divalent impurity ions diffuse rapidly along open channels parallel to the c-axis and are pushed into substitutional Ti sites by interstitial Ti ions. Divalent ions therefore have a large anisotropy in diffusion coefficient for different crystallographic directions. Trivalent and tetravalent ions dissolve substitutionally and diffuse interstitially. Both mechanisms are important for mixed-valent impurity ions such as Mn. However, in this system, the concentration gradient exists in the radial direction, orthogonal to the c-axis. Therefore it is likely that the diffusion of Mn from the shell into the wire core is driven by Mn atoms dissolving substitutionally and diffusing through an interstitial mechanism.[3] The larger diffusion coefficients observed for conversion in an Ar environment are a result of changes in point defect concentrations, namely oxygen vacancies and interstitial Ti atoms, with partial pressure of oxygen. In air, the diffusion coefficients are reduced due to the smaller point defect concentration and Mn is not reduced to the Mn^{2+} oxidation state as shown in XPS in Figure S13, however, the mechanism for diffusion is likely unchanged.

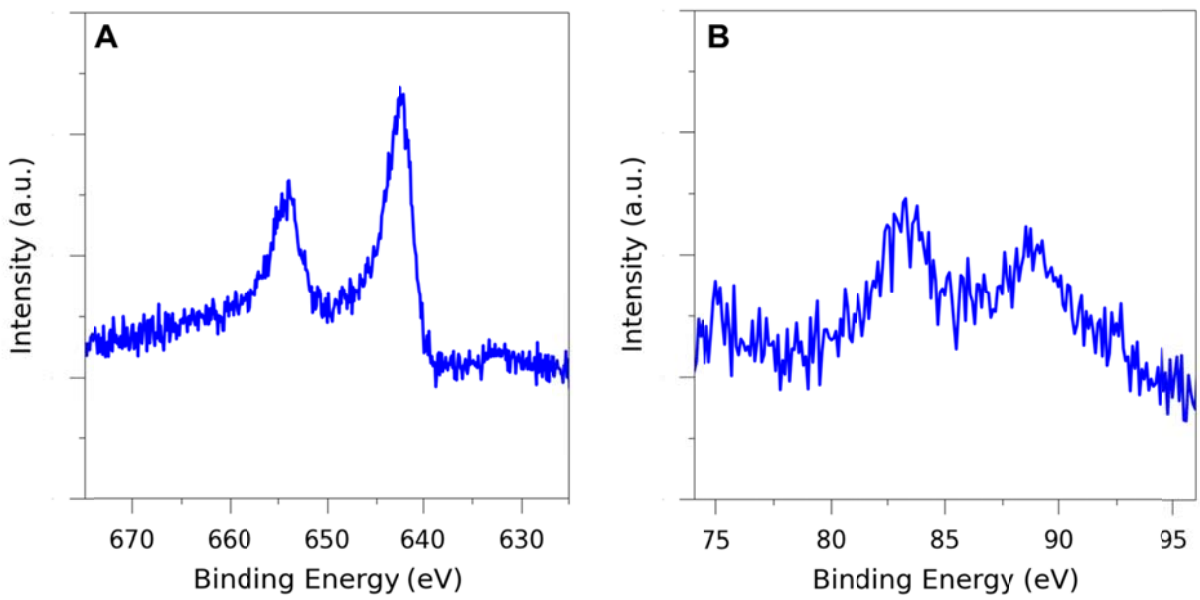

Figure S13: (A,B) XPS spectra of the Mn 2p and 3s regions, indicating the satellite peak distance in the 2p region and the 3s multiplet peak splitting. The values are consistent with a Mn^{3+} oxidation state.

References:

S1. Gorlin, Y.; Jaramillo, T. *J. Am. Chem. Soc.* **2010,** 132, 13612.

S2. Dicastro, V.; Polzonetti, G. *J. Electron Spectrosc. Relat. Phenom.* **1989,** 48, 117.

S3. Sasaki, J.; Peterson, N.; Hoshino, K. *J. Phys. Chem. Solids* **1985,** 46, 1267.